# Suppression of ferromagnetism and emergence of spin-glass-like behavior in the $CuCr_{2-x}Sn_xS_2Se_2$ spinels

Miguel Pardo-Sainz,[1,2] Silvana Moris,[3] Cristina Piquer,[1] José Alberto Rodríguez-Velamazán,[4] María Luisa López,[5] Inmaculada Álvarez-Serrano,[5] Antonio Galdámez,[6,*] and Javier Campo[1,7,†]

[1]*Instituto de Nanociencia y Materiales de Aragón (CSIC–Universidad de Zaragoza) and Departamento de Física de la Materia Condensada, C/Pedro Cerbuna 12, 50009 Zaragoza, Spain*

[2]*Graduate School of Science, Osaka Metropolitan University, 1-1 B4, Gakuenchou, Naka-ku, Sakai, Osaka 599-8531, Japan*

[3]*Centro de Investigación de Estudios Avanzados del Maule (CIEAM), Vicerrectoría de Investigación y Postgrado, Universidad Católica del Maule, Avenida San Miguel 3605, Talca 3480112, Chile*

[4]*Institut Laue-Langevin, 71 avenue des Martyrs, CS 20156, 38042 Grenoble Cedex 9, France*

[5]*Departamento de Química Inorgánica, Facultad de Ciencias Químicas, Universidad Complutense, 28040 Madrid, Spain*

[6]*Departamento de Química, Facultad de Ciencias, Universidad de Chile, Las Palmeras 3425, Ñuñoa, Santiago de Chile, Chile*

[7]*International Institute for Sustainability with Knotted Chiral Meta Matter (WPI-SKCM$^2$), Hiroshima University 1-3-1 Kagamiyama, Higashi-Hiroshima, Hiroshima 739-8526, Japan*

(Received 2 October 2023; revised 9 August 2024; accepted 15 August 2024; published 30 August 2024)

Magnetometry, neutron diffraction experiments, and high-resolution transmission electron microscopy (HRTEM) were performed to study the magnetic behavior of $CuCr_{2-x}Sn_xS_2Se_2$ ($0.2 \leqslant x \leqslant 1.0$) solid solutions and experimentally determine the appropriate magnetic structure for these systems. For all samples, the main phase with normal spinel-type structure ($Fd\bar{3}m$) was refined. For low Sn concentration a minority monoclinic phase appears also corroborated with HRTEM analyses. Together with the results from magnetization experiments, neutron diffraction measurements allowed to establish that for samples with $x \leqslant 0.4$ there is a ferromagnetic long-range order at high temperatures labeled with the $3d$ irrep $m\Gamma_4^+$ of $Fd\bar{3}m.1'$, while for $x > 0.4$ no magnetic signal is observed, indicating that the ferromagnetic behavior is suppressed and replaced with a spin-glass-like state.

DOI: 10.1103/PhysRevB.110.064436

## I. INTRODUCTION

The chalcogenide spinels with normal spinel-type structures $AB_2X_4$ have generated great interest because of their attractive physical properties, such as colossal magnetoresistance, multiferroicity, colossal magnetocapacitance, high thermoelectric performance, magnetic semiconducting properties, and spin-glass behavior, among other properties [1–7].

The physical and structural properties of these types of spinels are also strongly influenced by the distribution of the metal ions in the structure [4,8,9]. Because the cationic and anionic distributions can change when substitution occurs, the physical properties of these spinel materials may differ significantly from those of the end members [10–16]. Additionally, thiospinels and selenospinels can undergo pressure-induced phase transitions toward a monoclinic $Cr_3S_4$-type phase, accompanied by significant alterations in the magnetic and electronic properties [17–20].

Both the thiospinel $CuCr_2S_4$ and the selenospinel $CuCr_2Se_4$ have a normal spinel-type structure with space group (SG) $Fd\bar{3}m$ and high ferromagnetic (FM) Curie temperatures $T_C$ of 377 and 430 K, respectively [21,22]. Their magnetic properties can be explained by the double-exchange model between $Cr^{3+}$ and $Cr^{4+}$ [23], in which the diamagnetic $Cu^+$ cations occupy the tetrahedral sites and the FM moment arises from a parallel alignment of the spins of $Cr^{3+}$ and $Cr^{4+}$ located at the octahedral sites [24–28]. This double-exchange interaction is also responsible for the metallic behavior observed in the electrical conductivity measurements [29–31].

Chemical substitution of the Cr sublattice with diamagnetic ions modifies the magnetic properties of $CuCr_2X_4$ ($X$ = S, Se). In $CuCr_{2-x}M_xX_4$ spinels, where $M = Sn^{4+}$ or $Ti^{4+}$, and Cu remains as a diamagnetic $Cu^+$ cation, an evolution from FM behavior to a spin-glass regime has been described in $CuCr_{2-x}Ti_xS_4$ [7], $CuCr_{2-x}Sn_xS_4$ [16], $CuCr_{2-x}Ti_xSe_4$ [32], and $CuCr_{2-x}Sn_xSe_4$ [14,33]. Such evolution is explained in terms of magnetic frustration, which is triggered by the chemical substitutions of chromium by the $M$ diamagnetic ions. Thus, in the previous magnetic dilutions the *randomness*, which is also, together with magnetic frustration, an important ingredient to explain the spin-glass-like behavior, is originated only at the magnetic sublattice.

Analogous behavior has been observed when simultaneously substituting the Cr and S in $CuCr_{2-x}Sn_xS_{4-y}Se_y$, and therefore creating *randomness* in both the magnetic sublattice and the exchange pathway networks. Thus, magnetometry measurements in $CuCr_{2-x}Sn_xS_2Se_2$ with $x = 0.2$ and 0.4 exhibited FM behavior, whereas antiferromagnetic (AF) one was

*Contact author: agaldamez@uchile.cl
†Contact author: javier.campo@csic.es

 

observed for the samples with $x = 0.6$, 0.8, and 1.0 [34]. The comparison of $\mu_{\text{theo}}$ obtained from density functional theory (DFT) calculations with the experimental data $\mu_{\text{eff}}$ on $CuCr_{2-x}Sn_xS_2Se_2$ demonstrated that Sn was a diamagnetic cation with a IV-oxidation state and $\mu_{\text{eff}}$ was in agreement with the expected for $(Cu^{1+})_{\text{tet}}[Cr^{3+}Cr^{4+}_{1-x}Sn^{4+}_x]_{\text{oct}}S_2Se_2$. DFT calculations suggested that the decrease in FM interactions, associated with the chemical substitution of Cr by Sn, stimulates the AF behavior.

Thus, the scope of this research is to understand the magnetic structures of the family $CuCr_{2-x}Sn_xS_2Se_2$ with $x = 0.2$, 0.3, 0.4, 0.6, 0.8, and 1.0. In this family the amount of Sn controls the degree of dilution of the magnetic sublattice, for a given substitution of S by Se equal to 0.5. To reach our goal, as a first step, it will be necessary to determine and refine the crystalline structures of each member of the family and to quantify the degree of *random* substitution of Cr by Sn and, also, at the same time to verify if the anionic sublattice (S/Se) is fully *random* as function of the Sn content for the given Se content of 0.5, i.e., if the proposed model of $(Cu^{1+})_{\text{tet}}[Cr^{3+}Cr^{4+}_{1-x}Sn^{4+}_x]_{\text{oct}}S_2Se_2$ is really satisfied or not. The employed experimental techniques will be ac and dc magnetization, variable temperature neutron powder diffraction experiments, and high-resolution electron microscopy.

## II. MATERIALS AND METHODS

Powder samples of $CuCr_{2-x}Sn_xS_2Se_2$ were prepared by directly combining high-purity elemental powders (99.99%, Aldrich) in stoichiometric amounts (∼0.5 g of compound). Powders were mixed manually in hexane with ∼5 wt.% excess of S and Se in an agate mortar and pestle. Then, mixed powders were pressed into round-shaped pellets at ∼10 kPa, sealed in evacuated quartz ampules and placed in a horizontal tubular programmable furnace. All processes were carried out under Ar atmosphere. The ampules were slowly heated from room temperature (RT) to 500 °C at a rate of 150 °C/h and maintained at this temperature for 2 h, then were heated to 850 °C at a rate of 60 °C/h and kept for 10 days. Finally, the ampules were slowly cooled down to RT at a rate of 60 °C/h.

Magnetic measurements were performed on pelletized powder samples using a physical property measurement system (PPMS-9T), manufactured by Quantum Design, in a temperature range from 5 to 300 K. Continuous susceptibility $\chi_{\text{dc}}(T) = M(T)/H$ measurements were obtained under the zero field cooling (ZFC) and field cooling (FC) protocols with applied magnetic field $H = 500$ Oe. Isothermal magnetization $M(H)$ data were collected at $T = 5$ K in a field range from 0 to 90 kOe. Hysteresis loops have been recorded at $T = 5$ K between 50 and −50 kOe.

In-phase ($\chi'$) and out-of-phase ($\chi''$) components of the ac susceptibility were measured using a superconducting quantum interference device (SQUID) magnetometer, manufactured by Quantum Design. The temperature dependence of the signal was measured between 5 and 300 K, with an ac amplitude of 4 Oe and exciting frequencies $f$ ranging between 1 and 10 kHz.

Neutron powder diffraction (NPD) experiments were carried out on the high-flux two-axis neutron diffractometer D1B of the Institut Laue-Langevin (ILL) in Grenoble, France. This instrument has a detector covering an angular range of 128° with a definition of 0.1°. A radial oscillating collimator (ROC) was installed in order to eliminate the spurious signals produced by the sample environment. Data acquisitions were taken with two different neutron wavelengths, $\lambda = 1.28$ Å and 2.52 Å at several key temperatures in the range from 2 K to RT. For samples showing magnetic ordering, thermodiffractograms were collected with $\lambda = 2.52$ Å every 2 min as the samples were warmed up from 2 K to RT.

The Rietveld analysis of the diffraction data was performed with the help of the FULLPROF suite [35]. Several tools within the Bilbao Crystallographic Server (BCS) [36–39] were also employed for the symmetry analysis.

High-resolution transmission electron microscopy (HRTEM) was performed in a JEOL 300FEG. The composition of the obtained materials was established by semiquantitative chemical analysis using energy dispersive x-ray spectroscopy (EDXS). The samples were prepared by crushing the powders under *n*-butanol and dispersed over nickel grids covered with a porous carbon film.

## III. MAGNETIC MACROSCOPIC CHARACTERIZATION

### A. dc susceptibility

Figure 1 shows the $\chi_{\text{dc}}(T)$ curves measured for all $CuCr_{2-x}Sn_xS_2Se_2$ samples under ZFC and FC protocols with $H = 500$ Oe. Although the shape of the ZFC $\chi_{\text{dc}}(T)$ curves change with the Sn concentration, they all present a common phenomenology: from 300 K, when lowering $T$, they display first an increase at $T_1$ followed by a drop at $T_2$ (more pronounced in the ZFC branch). $T_1$ was determined as the minimum of the derivative $d\chi_{\text{dc}}(T)/dT$, while $T_2$ was determined as the maximum of $\chi_{\text{dc}}(T)$ (see Fig. 1). Moreover, at $T_{\text{Irr}}$, which is very close to $T_2$ for low fields, an irreversibility between the ZFC/FC curves takes place, even for $x = 0.2$ (see inset of Fig. 1).

The inverse susceptibility dependence at high temperatures was fitted to the Curie-Weiss law $\chi^{-1} = (T - \theta_{\text{CW}})/C$, where $C$ is the Curie constant and $\theta_{\text{CW}}$ the Curie-Weiss temperature (see insets of Fig. 1). From the fitted value of $C$ we can obtain the effective experimental magnetic moment for the Cr ions as $\mu_{\text{eff}} = \mu_{\text{B}}\sqrt{3k_{\text{B}}C/N_{\text{A}}} \approx \sqrt{8C}$. The theoretical effective magnetic moment, $\mu_{\text{theo}}$, has been calculated as

$$\mu_{\text{theo}} = \sqrt{\mu^2_{Cr^{3+}} + (1-x)\mu^2_{Cr^{4+}}},$$

where $\mu^2_{Cr^{3+/4+}} = g^2_{Cr^{3+/4+}} S_{Cr^{3+/4+}}(S_{Cr^{3+/4+}} + 1)$ is the theoretical effective magnetic moment for $Cr^{3+/4+}$. The Landé factors and spin values are $g_{Cr^{3+}} = 2$, $g_{Cr^{4+}} = 1.86$, $S_{Cr^{3+}} = \frac{3}{2}$, and $S_{Cr^{4+}} = 1$. The values of $\mu_{\text{theo}}$, together with the experimental data $T_1$, $T_2$, $T_{\text{Irr}}$, and the parameters $\theta_{\text{CW}}$ and $\mu_{\text{eff}}$ obtained from the fits, are summarized in Table I.

Isothermal magnetization $M(H)$ data were collected for $CuCr_{2-x}Sn_xS_2Se_2$ samples at $T = 5$ K in a field range from 0 to 90 kOe. These curves are shown in Fig. 2(a). A clear evolution is observed as the content of Sn, $x$, replacing the octahedral Cr site is increased. A very small hysteresis is also observed at the full cycle at 5 K for the $x = 0.3$ compound, as can be seen in Fig. 2(b).

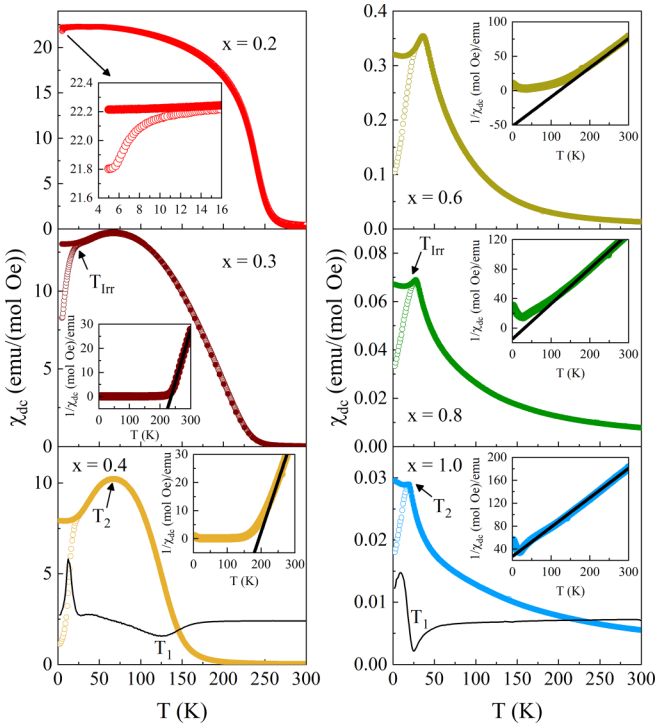


FIG. 1. Zero field cooled (ZFC) (open symbols) and field cooled (closed symbols) dc susceptibility curves measured at 500 Oe for powder samples with $x = 0.2$, 0.3, 0.4, 0.6, 0.8, and 1.0. The inset of $x = 0.2$ is a detailed view of the low-$T$ region of the ZFC and FC curves. The insets of $x = 0.3$, 0.4, 0.6, 0.8, and 1.0 show the inverse dc susceptibility and the corresponding Curie-Weiss law fit. In the compounds $x = 0.4$ and 1.0 the derivative $d\chi_{dc}/dT$ has been included (black line) to show how $T_1$ is determined. The irreversibility in the ZFC and FC curves $T_{Irr}$ is also signaled for the compounds $x = 0.3$ and 0.8.

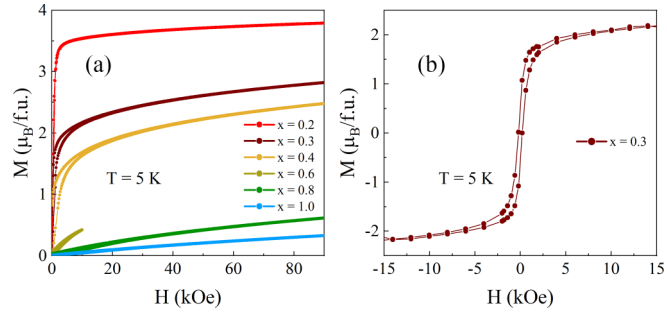


FIG. 2. (a) Isothermal magnetization $M(H)$ data at 5 K for $x = 0.2$, 0.3, 0.4, 0.6, 0.8, and 1.0. (b) Hysteresis cycle for $x = 0.3$.

For the minimum studied Sn substitution $x = 0.2$, we can observe that the dc susceptibility suddenly increases at $T_1 = 240$ K, while its magnetization isotherm saturates at high fields. Moreover, the high-temperature fit of the inverse of the dc susceptibility gives a positive value for the Curie-Weiss temperature $\theta_{CW}$ close to the value of $T_1$. Hence, the sample $CuCr_{1.8}Sn_{0.2}S_2Se_2$ behaves mostly as a ferromagnet, and $T_1$ can be considered as a Curie temperature. However, looking more closely, we appreciate some discrepancies regarding the FM behavior: at low temperatures (≈7 K) there is a small irreversibility in the ZFC and FC curves and the magnetization at saturation condition $3.8\,\mu_B$ is relatively small compared with the calculated magnetization $4.49\,\mu_B$. As we will discuss later in detail, these small discrepancies with respect to a ferromagnet behavior could be explained by considering the existence of AF interactions between $Cr^{3+}$ cations. The competition between ferromagnetic ($Cr^{3+} - Cr^{4+}$) and antiferromagnetic ($Cr^{3+} - Cr^{3+}$) interactions is one of the key ingredients for the appearance of a spin-glass behavior, which will be responsible for both the appearance of irreversibility in the ZFC and FC curves and the low values of the saturation magnetization [7,40,41].

The small irreversibility could also be assigned to the movement of magnetic domain walls in consonance with the weak hysteresis detected in the curve $M(H)$ at low temperatures and magnetic fields, for samples with $x = 0.2$, 0.3, and 0.4. The possibility of powder sample rotation is ruled out, as precautions were taken by using cotton to secure the powder within the magnetometer sample holder (capsule), and the magnetic field strength remains within acceptable limits.

The small value found in the magnetization saturation could also be justified by an itinerant electron ferromagnetism model due to double-exchange interactions. In this context, the magnetization saturation tends to be lower than expected in a localized spin model. However, the decrease of saturation value in $M(H)$ and the increase of the slope at high fields as we increase the value of $x$ to 0.3 and 0.4 would indicate a stronger itinerant behavior, which is in direct contradiction with the $Cr^{3+} - Cr^{4+}$ double-exchange interactions becoming weaker.

For intermediate Sn concentration samples $x = 0.3$ and 0.4, there is a significant change in the shape of the dc susceptibility curves, which begin to deviate appreciably from what is expected in an typical ferromagnet. Mainly, $T_1$ is significantly reduced (from 240 to 125 K), while the susceptibility decreases below $T_2$, the irreversibility at low $T$ is enhanced,

TABLE I. Values of $T_1$, $T_2$, $T_{Irr}$, $\theta_{CW}$, and experimental ($\mu_{eff}$) and theoretical ($\mu_{theo}$) effective magnetic moments obtained from the fits for the different samples of $CuCr_{2-x}Sn_xS_2Se_2$ phases. The superscript dagger (†) reflects data from Ref. [34].

| Sample | $x$ | $T_1$ (K) | $T_2$ (K) | $T_{Irr}$ (K) | $\theta_{CW}$(K) | $\theta_{CW}$(K)† | $\mu_{eff}$ ($\mu_B$) | $\mu_{eff}$ ($\mu_B$)† | $\mu_{theo}$ ($\mu_B$) |
|---|---|---|---|---|---|---|---|---|---|
| $CuCr_{1.8}Sn_{0.2}S_2Se_2$ | 0.2 | 240(2) | | 10(2) | +262(2) | +261.27 | 5.1(3) | 4.97 | 4.53 |
| $CuCr_{1.7}Sn_{0.3}S_2Se_2$ | 0.3 | 200(10) | 67(2) | 24(2) | +234(2) | | 4.4(3) | | 4.45 |
| $CuCr_{1.6}Sn_{0.4}S_2Se_2$ | 0.4 | 125(5) | 67(2) | 26(2) | +197.7(3) | +189.44 | 4.6(1) | 4.69 | 4.38 |
| $CuCr_{1.4}Sn_{0.6}S_2Se_2$ | 0.6 | 45(3) | 36(1) | 27(1) | +135.3(3) | +111.47 | 4.27(6) | 4.49 | 4.22 |
| $CuCr_{1.2}Sn_{0.8}S_2Se_2$ | 0.8 | 32(2) | 28(1) | 25(1) | +44.4(1) | +29.46 | 4.21(9) | 4.12 | 4.05 |
| $CuCr_{1.0}Sn_{1.0}S_2Se_2$ | 1 | 25(2) | 19(1) | 18(1) | −41.5(1) | −36.00 | 4.0(1) | 3.99 | 3.87 |

and the $M(H)$ curve no longer saturates. However, the compound still exhibits some of the hallmarks of a ferromagnet: namely, the shape of the $1/\chi_{dc}$ curve, the small hysteresis at $M(H)$, and the positive value of $\theta_{CW}$ (although in these cases it is significantly higher than $T_1$). Therefore, in these intermediate Sn concentration samples the exchange interactions have a dominant FM character but superposed with AF interactions, with the latter ones becoming more relevant as the concentration increases. In this context, $T_2$ would be the equivalent of a freezing temperature, $T_2 = T_f$.

For relatively high Sn concentration samples $x = 0.6$ and 0.8, the shapes of the magnetization curves clearly differ from those of a ferromagnet. The dc susceptibility curves display a sharper maximum at $T_2$, a strong ZFC and FC irreversibility, and the ZFC branches abruptly decrease towards zero for $T < T_{Irr}$. In $1/\chi_{dc}$ a small turn up is observed at low $T$. Moreover, the magnetization isotherms display a linear increase with the applied field and the magnetization at $T = 5$ K and $H = 90$ kOe has drastically decreased (from 3.8 to 0.6 $\mu_B$ for $x = 0.2$ and 0.8, respectively). Taking into account the increasingly small values of $T_1$ and $\theta_{CW}$, and the linear increase of the magnetization curves with the applied field, this suggests that the AF interactions are playing a major role in these systems. In this case, $T_1$ cannot be seen as a true Curie temperature, whereas $T_2$ does seem to correspond to a freezing temperature as in the previous compounds.

Finally, for $x = 1$, although the shape of the $\chi_{dc}(T)$ and $M(H)$ curves are very similar to those of 0.8, there is a fundamental difference: the $\theta_{CW}$ has become negative, which means that the interactions are predominantly AF in nature. This is also reflected in the form of the $1/\chi_{dc}$ curve, which is typical of an antiferromagnet.

As we can observe from Table I, these results are in agreement to those of the previously published for $CuCr_{2-x}Sn_xS_2Se_2$ phases and confirm the reproducibility of the magnetic measurements [34]. A good agreement is also obtained for the values of the effective magnetic moments when compared with the theoretical values expected for $Cu^{+}[Cr_1^{3+}Cr_{1-x}^{4+}Sn_x^{4+}]S_2Se_2$, confirming that Cu and Sn show diamagnetic behavior with I and IV oxidation states, respectively.

### B. ac susceptibility

Representative ac susceptibility curves for the compounds $CuCr_{1.7}Sn_{0.3}S_2Se_2$ ($x = 0.3$) and $CuCr_{1.6}Sn_{0.4}S_2Se_2$ ($x = 0.4$) are displayed in Fig. 3. The in-phase $\chi'(T)$ curves behave similar to the ZFC dc susceptibility, i.e., an increase at $T_1$ and a subsequent fall at $T_2$. An additional shoulder is also present at lower temperatures, which is better observed for $x = 0.3$. Regarding the out-of-phase component $\chi''(T)$, the $x = 0.3$ curve shows two broad peaks at the temperatures labeled $T_1^{ac} = 185(10)$ K and $T_2^{ac} = 83(2)$ K, and a well-defined peak at $T_3^{ac} = 21(2)$ K for the lowest frequency measured $f = 0.9$ Hz [see Fig. 3(a)]. The same qualitative behavior is observed for $x = 0.4$, where three well-defined peaks are located at $T_1^{ac} = 145(5)$ K, $T_2^{ac} = 69(2)$ K, and $T_3^{ac} = 31(2)$ K for the lowest frequency measured $f = 10$ Hz [see Fig. 3(b)]. Comparing these temperatures with the ones determined from the dc susceptibility, a clear correspondence

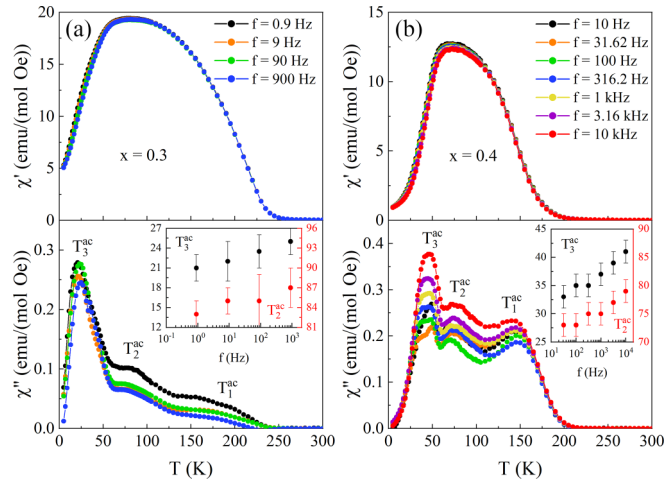


FIG. 3. ac magnetic susceptibility [$\chi'(T)$ and $\chi''(T)$] curves for $CuCr_{2-x}Sn_xS_2Se_2$ samples with $x = 0.3$ (a) and 0.4 (b). The peaks of the out-of-phase component $\chi''(T)$ are labeled for clarity. The insets display the frequency dependence of $T_2^{ac}$ and $T_3^{ac}$ for $x = 0.3$ (a) and $x = 0.4$ (b).

can be established. The Curie temperature $T_1$ corresponds with the first peak in $\chi''(T)$ at $T_1^{ac}$, which shows no frequency dependence. The broad peak at $T_2^{ac}$ roughly coincides with the maximum of the in-phase component and dc susceptibility curves ($T_2$) and has a clear frequency dependence in both $\chi'(T)$ and $\chi''(T)$, displayed in the insets of Fig. 3. Finally, the sharp peak at $T_3^{ac}$ correlates with the shoulder of the in-phase component and the splitting temperature between the ZFC and FC dc susceptibility curves ($T_{Irr}$), and also displays a clear frequency dependence. The linear relation between the logarithm of the applied frequency and the temperatures $T_2^{ac}$ and $T_3^{ac}$ further supports the freezing of the magnetic moments at low temperatures [32,40,42].

## IV. NEUTRON POWDER DIFFRACTION EXPERIMENTS

### A. Nuclear structure

Neutron powder diffraction (NPD) data were collected with $\lambda = 1.28$ Å at different temperatures between 2 K and RT for powder samples of $CuCr_{2-x}Sn_xS_2Se_2$ with $x = 0.2$, 0.3, 0.4, 0.6, 0.8, and 1.0. Some representative patterns are shown in Fig. 4 for all samples.

The Bragg peaks observed in samples labeled with $x = 0.6$, 0.8, and 1.0 can all be indexed by the same cubic crystal structure with SG $Fd\bar{3}m$ (No. 227) and no evidence of magnetic long-range order (LRO) is found down to the lowest measured temperature. Meanwhile, at RT the samples $x = 0.2$, 0.3, and 0.4 show the same Bragg peaks corresponding to a main cubic phase with SG $Fd\bar{3}m$ plus some additional peaks (marked by red asterisks in Fig. 4). Furthermore, as the temperature is decreased, an extra peak is observed for $x = 0.2$ and 0.3 at $Q \sim 1.08$ Å$^{-1}$, which suggests the development of some magnetic LRO. In the sample with $x = 0.4$, this peak shows a weak intensity at 100 K, and is not distinguishable at lower temperatures, implying that the magnetic LRO disappears as the temperature is decreased.

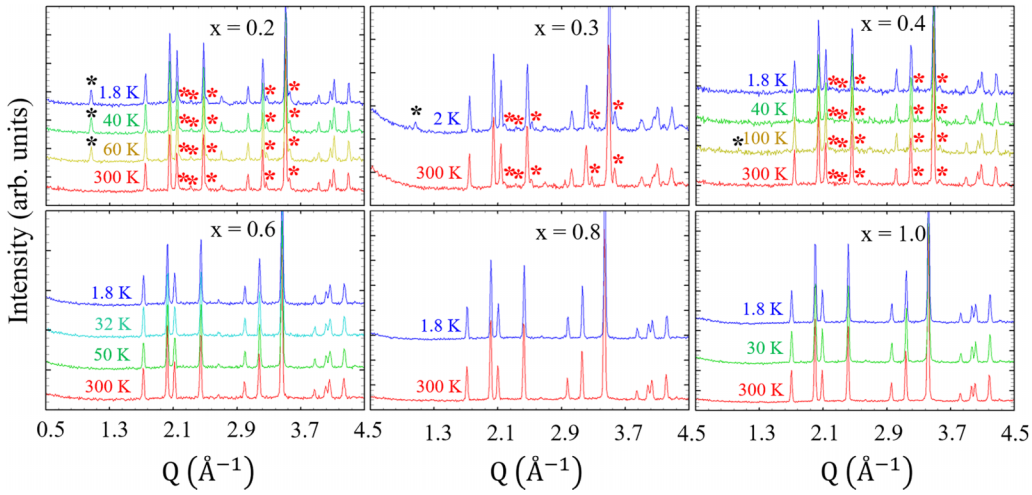


FIG. 4. Low-$Q$ region of some representative powder diffraction patterns collected with $\lambda = 1.28$ Å at different temperatures for powder samples of $CuCr_{2-x}Sn_xS_2Se_2$ with $x = 0.2$, 0.3, 0.4, 0.6, 0.8, and 1.0. The additional Bragg peaks, indexed by a monoclinic phase, are marked with red asterisks. The magnetic peak observed for $x = 0.2$, 0.3, and 0.4 is marked with a black asterisk.

For all samples, the main phase with normal spinel-type structure was refined by means of the Rietveld method. We considered that the tetrahedral sites, Wyckoff position (WP) 8*a*, were occupied by Cu and the octahedral ones (WP 16*d*) by $Sn^{4+}$, $Cr^{3+}$, and $Cr^{4+}$. Nevertheless, other models were also considered regarding the distribution of the Sn cation in the octahedral sites, however, the best result was obtained when both the Cr and Sn cations were randomly distributed on WP 16*d*, as observed in $CuCr_{2-x}Sn_xS_4$ [16], $CuCr_{2-x}Sn_xSe_4$ [33], $CuCr_{2-x}Sn_xS_{4-y}Se_y$ [34], and similar Hf-doped $CuCr_2Se_4$ spinels [15]. The S and Se atoms occupied the WP 32*e* with atomic coordinates ($u$ $u$ $u$), where the best model also corresponded with a random distribution of both anions. This can be expected since the effective ionic radii of $S^{2-}$ and $Se^{2-}$ are very similar (1.84 and 1.98 Å, respectively [43]). We constrained the occupancy of the WP 16*d* according to $(2-x)$ Cr + $x$ Sn and the one for the chalcogenides to $(4-y)$ S + $y$ Se. The refined values of $x$ and $y$ ($x_{\text{ref}}$ and $y_{\text{ref}}$) did not differ greatly from the nominal ones ($x_{\text{nom}}$) and are shown in Table II. Equivalent and isotropic Debye-Waller factors were considered for all the atoms at each given WP.

The model under consideration fits well the diffractograms, as can be observed in Fig. 5(a), where the experimental and calculated NPD profile of $CuCr_{2-x}Sn_xS_2Se_2$ sample with $x = 1.0$ at 300 K is shown. The parameters obtained from the Rietveld refinement for all the samples are listed in Table II. The obtained value of the cell parameter $a$ for $x = 1.0$ had an intermediate value between those of $CuCrSnS_4$ [44] and $CuCrSnSe_4$ [45], similar to the values reported for $(Cu)_{\text{tet}}[Cr_{2-x}Sn_x]_{\text{oct}}S_{4-y}Se_y$ spinels [34]. This intermediate value supports the random distribution of S and Se anions. As the content $x$ of Sn is decreased, the cell parameter $a$ decreases linearly and obeys the Vegard's law (see inset in top of Fig. 5). Such behavior can be understood by considering that the $Cr^{4+}$ ions are replaced by the larger $Sn^{4+}$ cations (effective octahedral ionic radii of $Cr^{4+}$ and $Sn^{4+}$ are 0.55 and 0.69 Å, respectively [43]). As can be observed in Table II, the cell parameter $a$ increases with increasing temperature for all $CuCr_{2-x}Sn_xS_2Se_2$ samples.

For the $x = 1.0$ sample, the $u$ parameter of the atomic position ($u$ $u$ $u$) of the chalcogenide at the WP 32*e* is $u = 0.2543(1)$, which is in good agreement with the value obtained in $CuCr_{1.1}Sn_{0.9}S_{2.3}Se_{1.7}$, $u = 0.25484(4)$ [46].

For the $x = 0.2$, 0.3, and 0.4 samples the additional Bragg peaks (labeled with red asterisks in Fig. 4) are indexed by a monoclinic unit cell. An example is shown in Fig. 5(b), where the fit to the full diffraction pattern of $x = 0.2$ at 1.8 K is shown. Unfortunately, these peaks have considerable small intensity and appear next to Bragg peaks of the main cubic structure, which prevented the determination of the monoclinic space group unequivocally. Nevertheless, by performing LeBail fits, we determined the unit cell parameters, which are shown in Table III.

### B. Magnetic structure

The inset in Fig. 5(b) shows the two-dimensional (2D) plots of the thermodiffractograms collected at $\lambda = 2.52$ Å for $x = 0.2$ and 0.3. From them we can follow the evolution with temperature of the intensity of the magnetic peak marked with a black asterisk in Fig. 4 and estimate the onset of the magnetic ordering at $T_C \approx 220(10)$ and 200(5) for $x = 0.2$ and 0.3, respectively. These values agree well with the ones obtained from the magnetization measurements ($T_1 = 240$ and 200 K for $x = 0.2$ and 0.3, respectively).

The presence of this magnetic peak, as well as the increase in intensity of some nuclear peaks for the samples $x = 0.2$, 0.3, and 0.4, can be indexed by a propagation vector $\vec{k} = (0\,0\,0)$. We can decompose the magnetic representation for the Cr atom, located at WP 16*d*, as a direct sum of irreducible representations (irreps) of the parent group $Fd\bar{3}m.1'$ for the Γ point, (0 0 0), of the Brillouin zone (BZ), as follows:

$$m\Gamma_{16d} = 1m\Gamma_2^+(1) \oplus 1m\Gamma_3^+(2) \oplus 2m\Gamma_4^+(3) \oplus 1m\Gamma_5^+(3).$$

After a systematic trial and error procedure, the magnetic peak was correctly fitted by the 3*d* irrep $m\Gamma_4^+$ [see Fig. 5(b)], which is also the only irrep which allows a FM order, in agreement with the magnetization measurements shown previously in

TABLE II. Structural parameters obtained from Rietveld refinement of NPD patterns for the family $CuCr_{2-x}Sn_xS_{4-y}Se_y$.

| Cubic phase | | | | | | | | | |
|---|---|---|---|---|---|---|---|---|---|
| $T$ (K) | $a$ (Å) | $u$ | $B_{ISO}$(Cu) | $B_{ISO}$(Cr/Sn) | $B_{ISO}$(S/Se) | $x_{ref}$ | $y_{ref}$ | $R_{Bragg}$ | $\mu_{Cr}$ ($\mu_B$) |
| $CuCr_{1.8}Sn_{0.2}S_2Se_2$ ($x_{nom} = 0.2$, $y_{nom} = 2$) | | | | | | | | | |
| 300 | 10.0906(1) | 0.7440(2) | 1.73(7) | 1.0(1) | 1.14(5) | 0.18(5) | 1.96(2) | 3.42 | |
| 60 | 10.0791(1) | 0.7439(2) | 1.42(5) | 0.85(7) | 0.94(3) | 0.18 | 1.96 | 2.20 | 2.33(5) |
| 40 | 10.0789(1) | 0.7434(2) | 1.31(6) | 0.82(8) | 1.02(4) | 0.18 | 1.96 | 1.54 | 2.36(5) |
| 1.8 | 10.0791(1) | 0.7439(2) | 1.47(6) | 0.32(7) | 0.82(3) | 0.18 | 1.96 | 2.16 | 2.39(5) |
| $CuCr_{1.7}Sn_{0.3}S_2Se_2$ ($x_{nom} = 0.3$, $y_{nom} = 2$) | | | | | | | | | |
| 300 | 10.1309(2) | 0.7434(3) | 3.9(1) | 2.2(1) | 2.47(8) | 0.28(5) | 1.93(2) | 5.31 | |
| 2 | 10.1189(2) | 0.7446(4) | 2.9(1) | 1.8(1) | 1.95(7) | 0.28 | 1.93 | 3.91 | 1.1(1) |
| $CuCr_{1.6}Sn_{0.4}S_2Se_2$ ($x_{nom} = 0.4$, $y_{nom} = 2$) | | | | | | | | | |
| 300 | 10.1595(1) | 0.7435(2) | 2.39(8) | 1.7(1) | 1.88(6) | 0.37(5) | 2.02(2) | 1.75 | |
| 100 | 10.1451(1) | 0.7445(3) | 1.93(9) | 0.9(1) | 1.58(5) | 0.37 | 2.02 | 2.44 | 0.4(3) |
| 40 | 10.1444(1) | 0.7439(2) | 1.95(8) | 0.88(9) | 1.44(5) | 0.37 | 2.02 | 2.67 | |
| 1.8 | 10.1443(1) | 0.7440(2) | 1.81(8) | 1.01(9) | 1.36(4) | 0.37 | 2.02 | 2.91 | |
| $CuCr_{1.4}Sn_{0.6}S_2Se_2$ ($x_{nom} = 0.6$, $y_{nom} = 2$) | | | | | | | | | |
| 300 | 10.2270(1) | 0.7451(2) | 2.18(7) | 1.1(1) | 1.39(5) | 0.63(5) | 1.98(2) | 5.43 | |
| 50 | 10.2112(1) | 0.7447(2) | 1.41(5) | 0.65(6) | 0.97(3) | 0.63 | 1.98 | 4.91 | |
| 32 | 10.2113(1) | 0.7453(2) | 1.44(6) | 0.64(6) | 1.04(3) | 0.63 | 1.98 | 5.68 | |
| 1.8 | 10.2115(1) | 0.7446(2) | 1.45(5) | 0.69(6) | 0.93(3) | 0.63 | 1.98 | 5.20 | |
| $CuCr_{1.2}Sn_{0.8}S_2Se_2$ ($x_{nom} = 0.8$, $y_{nom} = 2$) | | | | | | | | | |
| 300 | 10.29635(9) | 0.7454(2) | 2.41(5) | 1.13(5) | 1.32(4) | 0.80(2) | 1.94(2) | 4.77 | |
| 1.8 | 10.27778(9) | 0.7453(1) | 1.46(4) | 0.55(4) | 0.90(2) | 0.80 | 1.94 | 4.92 | |
| $CuCrSnS_2Se_2$ ($x_{nom} = 1.0$, $y_{nom} = 2$) | | | | | | | | | |
| 300 | 10.35932(7) | 0.7457(1) | 2.38(4) | 0.96(5) | 1.22(3) | 1.05(2) | 1.96(2) | 3.67 | |
| 30 | 10.34047(8) | 0.7455(1) | 1.52(4) | 0.55(4) | 0.83(2) | 1.05 | 1.96 | 3.81 | |
| 1.8 | 10.34075(8) | 0.7457(1) | 1.55(4) | 0.57(4) | 0.82(2) | 1.05 | 1.96 | 3.41 | |

Figs. 1 and 2. In order to obtain more information about the real symmetry of this magnetic phase we employed the k-SUBGROUPSMAG tool of the BCS which provides with the isotropy subgroups of the parent group $Fd\bar{3}m.1'$ that are compatible with the $m\Gamma_4^+$ as a primary irrep. Following this procedure six isotropy subgroups were found ($R\bar{3}m'$, $I4_1/am'd'$, $Imm'a'$, $C2'/c'$, $C2'/m'$, and $P\bar{1}$), each of them with a different order-parameter direction. However, we could not determine which magnetic space group describes the symmetry of the system since all the isotropy subgroups fitted successfully the data and we do not have additional information about the direction of the order parameter (magnetic measurements were performed on powder samples, due to the difficulty to grow enough size single crystals).

Nevertheless, all the magnetic models converge to the same value for the modulus of the Cr magnetic moment, which is shown in Table II for each sample. For $x = 0.2$, the cation ordering model $Cu^+[Cr_{1.0}^{3+}Cr_{0.8}^{4+}Sn_{0.2}^{4+}]S_2Se_2$ predicts the determined value of 2.39(5) $\mu_B$. For the $x = 0.3$ and 0.4 samples, the values of the magnetic moment obtained from the refinement are reduced to 1.1 $\mu_B$ and 0.4 $\mu_B$, respectively. It should be noted that the magnetic signal observed in the NPD data reflects only the average of the long-range-ordered magnetic moments. Hence, these results agree well with our hypothesis of having a nearly or completely glassy system at low $T$, when the AF frustrated interactions developed for higher Sn content weaken the dominant FM interactions.

On the other hand, we do not observe any change in the intensity of the peaks indexed by the monoclinic phase (red asterisks in Fig. 4) with the temperature, which implies negligible magnetic ordering in this secondary phase.

## V. HIGH-RESOLUTION TRANSMISSION ELECTRON MICROSCOPY

In order to determine if the peaks indexed by the monoclinic phase correspond to a impurity phase or to a structural phase transition, the microstructural features of $CuCr_{2-x}Sn_xS_2Se_2$ ($x = 0.2$, 0.3, and 0.4) were studied by using HRTEM. Representative microcrystals with undefined morphology formed by very narrow crystals which are pilled and caked are shown in Fig. 6.

Most crystals could be analyzed in terms of the cubic spinel-type structure ($Fd\bar{3}m$). In Figs. 6(a)–6(d) observed distances of 2.1 and 3.8 Å between contrasts corresponding to (4 2 2) and (2 2 0) interplanar distances, respectively, can be appreciated. Typically, the observed most frequent orientation of the crystallites corresponds to the [1 1 1] zone axis. Besides,

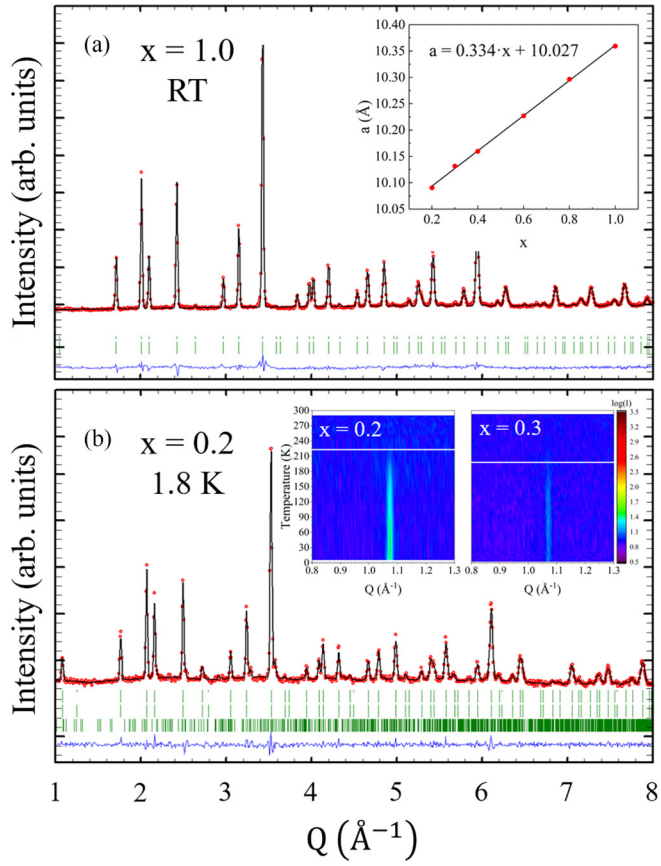


FIG. 5. Representative NPD profile of $CuCr_{2-x}Sn_xS_2Se_2$, $x = 1.0$ at 300 K (a) and $x = 0.2$ at 1.8 K (b). In red are shown the observed points and in black continuous line the calculated pattern with the parameters shown in Table II. The blue continuous line and the green ticks indicate the difference between the observed and calculated profiles and the position of nuclear and magnetic Bragg reflections of the spinel-type structure, respectively. The inset in (a) shows the evolution of the cell parameter $a$ versus $x$ values for $CuCr_{2-x}Sn_xS_2Se_2$ at RT, where the black line denotes the linear fit of the experimental data. The inset in (b) shows the 2D plots of the thermodiffractograms collected at 2.52 Å for $x = 0.2$ and 0.3. The evolution of the intensity of the magnetic peak marked with a black asterisk in Fig. 4 allows to estimate the onset of the magnetic ordering.

contrasts within small "wrinkle" regions are apparent (up to 8.4 Å), which could be an effect of disordered pilling of very thick crystals at the borders [high magnification image in the inset of Fig. 6(a)]. The mean composition from several microcrystals, measured in different points, is roughly concordant with the nominal one.

In addition, in all cases some microcrystals with different symmetry, not compatible with a cubic spinel-type lattice, were detected. Figures 6(e)–6(h) show representative images and electron diffraction (ED) patterns for such crystals. They could be indexed based on a monoclinic 4C $Fe_7S_8$-type structure [47], related to that of NiAs, with cell parameters $a \sim 2\sqrt{3}a_p$, $b \sim 2a_p$, $c \sim 4a_p$, being $a_p = 3.4$ Å. Thus, the observed distances of 5.1, 5.8, and 6.3 Å are assigned to the monoclinic $(2\ 0\ 0)_m$, $(1\ 1\ 0)_m$, and $(0\ 0\ 2)_m$, respectively. The cell parameter values are coherent with the ones obtained from the LeBail fits, confirming that the additional Bragg peaks correspond to a small secondary phase with different symmetry than the main cubic phase. Such phase probably also corresponds with the minor impurity phase observed in $CuCr_{1.6}Sn_{0.4}S_{2.3}Se_{1.7}$, which was suggested to affect the values of the electrical conductivity [46].

TABLE III. Lattice parameters obtained from by LeBail fits of NPD patterns for the family $CuCr_{2-x}Sn_xS_2Se_2$.

| Monoclinic phase | | | | | |
|---|---|---|---|---|---|
| $T$ (K) | $a$ (Å) | $b$ (Å) | $c$ (Å) | $\beta$ (deg) | $V$ (Å$^3$) |
| $CuCr_{1.8}Sn_{0.2}S_2Se_2$ | | | | | |
| 300 | 11.190(4) | 6.955(2) | 13.545(4) | 113.07(3) | 969.9(5) |
| 60 | 11.216(3) | 6.939(1) | 13.548(3) | 113.16(3) | 969.4(4) |
| 40 | 11.194(3) | 6.938(2) | 13.539(2) | 112.96(2) | 968.3(4) |
| 1.8 | 11.193(3) | 6.952(2) | 13.531(4) | 113.14(3) | 968.1(4) |
| $CuCr_{1.7}Sn_{0.3}S_2Se_2$ | | | | | |
| 300 | 11.177(1) | 6.957(1) | 13.512(3) | 113.22(1) | 965.5(3) |
| 2 | 11.166(1) | 6.962(1) | 13.549(2) | 113.06(1) | 969.1(2) |
| $CuCr_{1.6}Sn_{0.4}S_2Se_2$ | | | | | |
| 300 | 11.200(1) | 6.9690(9) | 13.610(2) | 113.453(8) | 974.6(2) |
| 100 | 11.197(4) | 6.975(2) | 13.587(4) | 113.43(3) | 973.7(6) |
| 40 | 11.185(5) | 6.982(2) | 13.582(5) | 113.35(3) | 973.8(6) |
| 1.8 | 11.185(4) | 6.982(3) | 13.568(5) | 113.30(3) | 973.2(6) |

## VI. DISCUSSION

### A. Sn content dependent magnetism

Taking into account the experimental results from both the magnetization and NPD measurements, a summary of the different magnetic phases observed as function of the Sn content is proposed in Fig. 7.

The results demonstrate a progressive change in the magnetic ground state of these compounds from a FM system, $CuCr_{1.8}Sn_{0.2}S_2Se_2$, to a spin-glass-like behavior in $CuCrSnS_2Se_2$, in which AF interactions prevail, but without any observed LRO. To understand the magnetic behavior in the family $CuCr_{2-x}Sn_xS_2Se_2$, we need to consider that $Cr^{3+} - Cr^{4+}$ interactions are FM (double exchange), while the $Cr^{3+} - Cr^{3+}$ ones are AF (superexchange). Moreover, it is important to note that the system presents a random magnetic dilution, i.e., each cation ($Cr^{3+}$, $Cr^{4+}$, and $Sn^{4+}$) is randomly connected with the others. Additionally, the Se and S anions are also randomly distributed, which will randomly modify the exchange pathways between the Cr cations.

When the amount of $Cr^{3+}$ and $Cr^{4+}$ cations in the system is the same (i.e.. $x = 0$, $CuCr_2S_2Se_2$), the probability to find connected FM Cr pairs is maximal (over the percolation threshold, $p = 0.401$, for an octahedral sublattice in the spinel [48]), the degree of frustration is low, and, therefore, it leads to a FM LRO. For low Sn content ($x = 0.2$, 0.3, and 0.4), the dominant interaction is still FM, establishing a LRO at $T_C$ confirmed by the onset of a magnetic peak in the NPD patterns. However, when Sn enters in the system, aside from the magnetic dilution effect, the AF interaction between $Cr^{3+}$

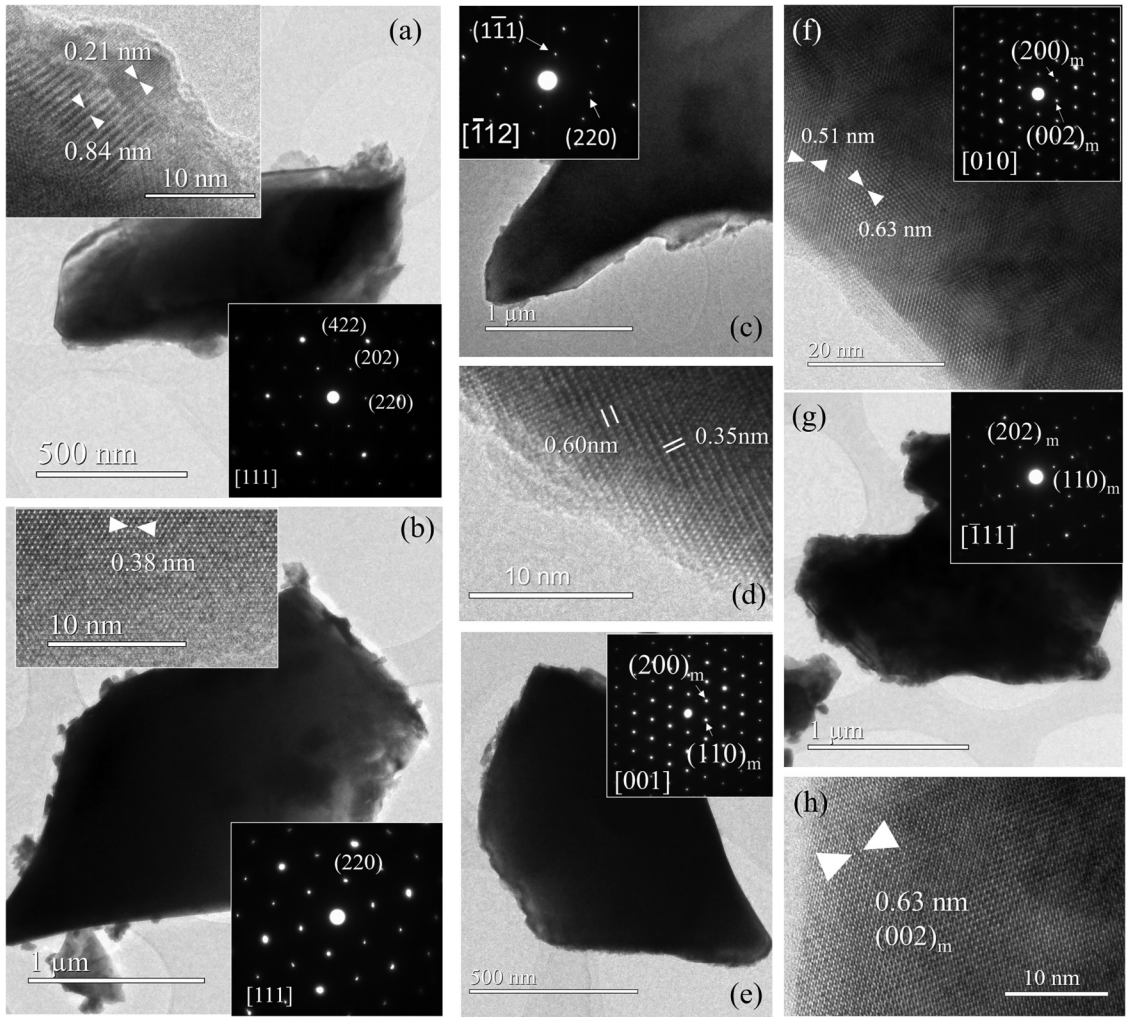


FIG. 6. HRTEM images and ED patterns for spinel-type $CuCr_{2-x}Sn_xS_2Se_2$ with cubic symmetry for $x = 0.2$ (a), 0.3 (b), 0.4 (c) and (d). HRTEM images and ED patterns for crystals indexed considering the monoclinic $Fe_7S_8$-type phase for $x = 0.2$ (e) and (h), 0.3 (f), 0.4 (g).

ions begins to grow at the expense of the FM one, which causes the increase of magnetic frustration and a blockage below $T_2$.

As the Sn content increases ($x = 0.6$, 0.8), although FM interactions are dominant ($\theta_{CW} > 0$) they do not percolate all over the system. In this case, $T_1$ is not a true Curie temperature, provided that although the system tends to order itself, the process is not completed at any time. As in the previous case, at low enough temperatures, magnetic frustration becomes dominant throughout the crystal, leading to the freezing of most of the magnetic moments at $T_2$. In this case the FM pairs are grouped in isolated clusters (far from the percolation threshold) resulting in some short-range order (SRO) at $T_1$.

For $x = 1$, only AF interactions are present among the $Cr^{3+}$ ions ($\theta_{CW} < 0$), however, the magnetic frustration and the dilution of the magnetic lattice with increasingly diamagnetic $Sn^{4+}$ cations hamper the development of any magnetic LRO. In this scenario, $T_1$ and $T_2$ almost merge and cannot be considered critical temperatures but rather represent the onset of some reminiscent short-range order (SRO) overimposed to a spin-glass-like behavior, compatible with the absence of any magnetic signals in the NPD data. A similar behavior has been reported in the parent compounds $CuCr_{2-x}Sn_xSe_4$, in which no dilution exists in the chalcogenide site [33].

The landscape explained in the precedent paragraphs would predict the decreasing of the electrical conductivity as the content of $Sn^{4+}$ increases, from a metallic behavior, when the sample is ferromagnetic, to an insulator, for the AF or spin-glass-like phase, due to the weakening of the $Cr^{3+} - Cr^{4+}$ double-exchange interactions. This is in agreement with the semiconducting behavior of the electrical conductivity measured for $CuCr_{2-x}Sn_xS_{2.3}Se_{1.7}$ and $CuCr_{2-x}Sn_xS_{1.7}Se_{2.3}$ ($x = 0.4$, 0.6, and 1.0) [46]. However, one should anticipate a metal-insulator transition occurring at intermediate compositions, which has not been measured yet.

Additionally, following the dependence of the Cr-Se/S bonds length with the Sn content, an increase is observed from 2.459 94(7) Å ($x = 0.2$) to 2.5418(14) Å ($x = 1.0$). Such increase in the bond length results in a weakening of the $Cr^{3+} - Cr^{4+}$ superexchange interaction, and therefore it stimulates the AF interactions [33]. This is observed in $CuCr_{2-x}Sn_xS_4$, where the smaller S anions give as a result shorter bonds and Curie-Weiss temperatures $\theta_{CW}$ for $x = 1$, 0.8 indicating a stronger FM contribution [16]. Thus, it seems that the effect

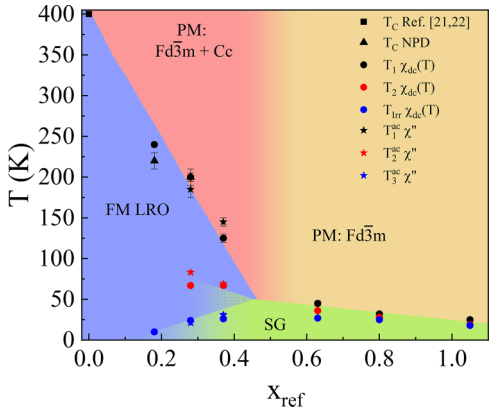


FIG. 7. Magnetic ground state versus the refined $x_{\text{ref}}$ value for the family $CuCr_{2-x}Sn_xS_2Se_2$ obtained by plotting the Curie temperature $T_C$ ($T_1$, $T_1^{ac}$) (black), the freezing temperature $T_f$ ($T_2$, $T_2^{ac}$) (red), and the irreversibility temperature $T_{Irr}$ ($T_3^{ac}$) (blue) determined from the analysis of dc susceptibility (filled circles), ac susceptibility (filled stars), and NPD (filled triangles) experiments. The $T_C$ for $x = 0$ is also plotted by averaging the values for $CuCr_2S_4$ and $CuCr_2Se_4$ from Refs. [21,22] (black filled square). The different magnetic phases present are labeled as paramagnetic (PM), ferromagnetic long-range order (FM LRO), spin-glass like (SG).

of the bond *randomness* is mainly due to the relative anion size and less important in determining the magnetic properties compared with the magnetic site *randomness*, as suggested by Belakroum *et al.* [42].

In particular, the complex behavior of the sample with $x = 0.4$ helps us to understand the magnetic behavior of the entire series. The existence of a tiny magnetic peak at 100 K in the NPD data implies the presence of FM LRO which is associated with the increase in the dc susceptibility curve at $T_1 = 125(5)$ K. Hence, for $x = 0.4$, $T_1$ is also a true Curie temperature, although only 0.4 $\mu_B$ are ordered due to the existence of frustration. At $T = 40$ K, the intensity of the magnetic peak is indistinguishable from the background contribution in the corresponding NPD diffractogram. Hence, the abrupt decrease in $\chi_{dc}(T)$ and the maximum in the out-of phase signal of the susceptibility $[\chi''(T)]$ observed below 70 K, characteristic of the reentrant spin glass [7,40], are associated with the loss of LRO. This might be explained assuming that for $x = 0.4$ Sn concentration, the probability to find a $Cr^{4+}$ as first neighbor (in a frustrated magnetic lattice with $3 + 3$ first neighbors) of a given $Cr^{3+}$ site is smaller than the probability to find another $Cr^{3+}$. If it is the case, the number of $Cr^{3+} - Cr^{3+}$ AF pairs with center in a given $Cr^{3+}$ respect the number of $Cr^{3+} - Cr^{4+}$ FM pairs will be larger, and therefore at low temperatures it might induce the creation of a spin-glass-like magnetic ground state. This could be in agreement with the fact that $\chi''(T)$ has a visible frequency dependence for $x = 0.4$ at low temperatures (see right side of Fig. 3). Finally, at 2 K the spin-glass state is already fully established in the whole system, causing the almost zero macroscopic magnetization as well as the absence of the NPD magnetic peak.

Special attention merits the region between $0.4 \leqslant x \leqslant 0.6$ in Fig. 7 in which the potential presence of a critical point at around $x \sim 0.5$ , where the PM, FM, and SG phases could coexist, cannot be discarded. Regarding from previous section that the increase in $x$ makes the monoclinic phase not energetically favorable anymore, our data appear to indicate some correlation between the absence of the monoclinic impurity and the appearance of SG state. However, at this stage more experimental work is needed to confirm this fact. For example, the evolution of the magnetic and nuclear structures as function of the pressure and the temperature.

A very similar magnetic phase diagram has been reported in $CuCr_{2-x}Ti_xS_4$ [7], where the ground state below $T_2$ was assumed to be a coexistence of the ferromagnetic and spin-glass states due to the freezing of the components of the magnetic moment perpendicular to the applied field, while the ground state below $T_{Irr}$ was described by a freezing of all spin components. If we assume such hypothesis, the lines defined by $T_2$ and $T_{Irr}$ could be explained by the G-T and A-T theories [49,50]. These lines vanish with a crossover behavior when the system approaches the FM LRO phase. Furthermore, Kariya *et al.* speculated about the out-of phase signal of the susceptibility $[\chi''(T)]$ exhibiting three characteristic temperatures [7], in perfect agreement with our results, which would corroborate the freezing of the transverse and longitudinal spin components at the G-T and A-T lines, respectively. However, a microscopic direct evidence of such freezing would be desirable. By following the intensity of the magnetic Bragg peaks and its surrounding background in NPD experiments with applied magnetic field, a confirmation of these ideas could be obtained.

### B. Monoclinic phase

The peaks indexed by the secondary monoclinic phase, confirmed by both NPD and HRTEM experiments, are similar to the ones reported for $CuCr_2Se_4$ measured under an applied pressure of 9.9 GPa [20]. In that study, they observed a cubic $Fd\bar{3}m$ to monoclinic structural transition which is completed at ~20 GPa. Although the space group was not determined due to significant overlap of adjacent Bragg peaks and high texture effects, the authors suggested that the system $CuCr_2Se_4$ transformed into a $CrMo_2S_4$-type structure with SG $Cc$, which in turn is a distorted variant of the $Cr_3S_4$-type phase (SG $C2/m$).

While all of the $ACr_2S_4$ sulfides ($A$ = Mn-Zn, Cd, Hg) crystallize in the cubic $Fd\bar{3}m$ structure [51], the vast majority of $ACr_2Se_4$ selenides favors the $Cr_3S_4$-type phase ($A$ = Mn-Ni), and only a few selenide materials adopt the cubic structure ($A$ = Cu, Zn, Cd, Hg) [17]. The comparison between both spinel families suggests that both the larger size and the more covalent character of $Se^{2-}$ favor the adoption of this monoclinic structure for magnetic $A$ cations. In addition, Efthimiopoulos *et al.* [20] argued that the $Fd\bar{3}m$ to monoclinic structural transition in $CuCr_2Se_4$ could be facilitated by the size similarity between the $Cu^+$ and $Cr^{3+}$ cations [$r(Cu^+) = 0.6$ Å and $r(Cr^{3+}) = 0.615$ Å [43]].

In our case, the system $CuCr_{2-x}Sn_xS_2Se_2$ with the chalcogenide site equally and randomly occupied by $S^{2-}$ and $Se^{2-}$ anions develops an energetically favorable impurity monoclinic phase. Taking into account the evolution of the unit-cell parameter $a$ with $x$ in Fig. 5(a), it can be deduced that the increase in content of Sn $x$ induces an expansion of the unit-cell

volume. Such expansion can be seen as an internal negative pressure acting on the system, which lowers its density and makes the monoclinic phase not energetically favorable anymore for high concentrations of Sn.

Therefore, although the experiments performed in this study for $CuCr_{2-x}Sn_xS_2Se_2$ were done at ambient pressure, a process involving chemical pressure due to the Sn incorporation could explain the Sn dependence of the monoclinic phase.

## VII. CONCLUSIONS

A new series of solid solution spinels with formula $CuCr_{2-x}Sn_xS_2Se_2$ ($0.2 \leqslant x \leqslant 1.0$) have been synthesized and studied with dc and ac magnetization, high-resolution transmission electron microscopy, and neutron powder diffraction experiments to study its magnetic behavior.

The crystalline structure of these series of spinels has been refined and a new unexpected secondary monoclinic phase has been manifested.

Regarding the magnetic properties of these compounds, our combined magnetometry and NPD diffraction study allow us to conclude that a progressive change in the magnetic ground state takes place, with the compounds evolving from a FM system, $CuCr_{1.8}Sn_{0.2}S_2Se_2$, to a spin-glass-like system $CuCrSnS_2Se_2$, in which AF frustrated interactions prevail, but without LRO. The magnetism of these compounds can be understood within the $Cu^{+}[Cr^{3+}_{1.0}Cr^{4+}_{1-x}Sn^{4+}_{x}]S_2Se_2$ model, in which a random competition between $Cr^{3+} - Cr^{4+}$ FM interactions (double exchange) and $Cr^{3+} - Cr^{3+}$ AF interactions (superexchange) takes place.

Our results allow to propose a FM LRO for $x \leqslant 0.4$ samples which can be classified under the irrep $m\Gamma^{+}_{4}$. In samples with relatively high Sn concentration ($x > 0.4$) the frustration and the random Sn diamagnetic dilution become dominant. In these compounds FM LRO is suppressed and replaced by a magnetic state compatible with a spin-glass-like behavior.

## ACKNOWLEDGMENTS

This work was supported by Grant No. PID2022-138492NB-I00-XM4 funded by MCIN/AEI/10.13039/501100011033, Grant Fondecyt Iniciación No. 11200126 from ANID, grants OTR02223-SpINS from CSIC/MICIN and DGA/M4 from Diputación General de Aragón. Beam time allocation trough the CRG-2712 experiment is also acknowledged. M.P.-S. acknowledges support from a Ph.D. fellowship from the Diputación General de Aragón (Spain).

[1] A. P. Ramirez, R. J. Cava, and J. Krajewski, Colossal magnetoresistance in Cr-based chalcogenide spinels, Nature (London) **386**, 156 (1997).

[2] J. Hemberger, P. Lunkenheimer, R. Fichtl, H.-A. K. von Nidda, V. Tsurkan, and A. Loidl, Relaxor ferroelectricity and colossal magnetocapacitive coupling in ferromagnetic $CdCr_2S_4$, Nature (London) **434**, 364 (2005).

[3] S. Krohns, F. Schrettle, P. Lunkenheimer, V. Tsurkan, and A. Loidl, Colossal magnetocapacitive effect in differently synthesized and doped $CdCr_2S_4$, Phys. B (Amsterdam) **403**, 4224 (2008).

[4] C. Bourgès, B. Srinivasan, B. Fontaine, P. Sauerschnig, A. Minard, J.-F. Halet, Y. Miyazaki, D. Berthebaud, and T. Mori, Tailoring the thermoelectric and structural properties of Cu-Sn based thiospinel compounds [ $CuM_{1+x}Sn_{1-x}S_4$ (M = Ti, V, Cr, Co)], J. Mater. Chem. C **8**, 16368 (2020).

[5] V. A. Fedorov, Y. A. Kesler, and E. G. Zhukov, Magnetic semiconducting chalcogenide spinels: Preparation and physical chemistry, Inorg. Mater. **39**, S68 (2003).

[6] H. Sims, K. Ramasamy, W. H. Butler, and A. Gupta, Electronic structure of magnetic semiconductor $CdCr_2Te_4$: A possible spin-dependent symmetry filter, Appl. Phys. Lett. **103**, 192402 (2013).

[7] F. Kariya, S. Ebisu, and S. Nagata, Evolution from a ferromagnetic to a spin-glass regime in the spinel-type, J. Solid State Chem. **182**, 608 (2009).

[8] J. Padiou, D. Bideau, and J. Troadec, Propriétés magnétiques et électriques de thiospinelles quaternaires, J. Solid State Chem. **31**, 401 (1980).

[9] F. Ozel, H. Kılıc, H. Coskun, I. Deveci, A. Sarılmaz, A. Balıkcıoglu, Y. Gundogdu, A. Aljabour, A. Ozen, S. Gezgin, A. Houimi, A. Yar, M. Kus, and M. Ersoz, A general review on the thiospinels and their energy applications, Mater. Today Energy **21**, 100822 (2021).

[10] M. Gogoowicz, S. Juszczyk, J. Warczewski, and T. Mydlarz, Ferrimagnetism of $Cu_{0.45}Co_{0.55}Cr_2S_{4-y}Se_y$, Phys. Rev. B **35**, 7073 (1987).

[11] S. Tsuji, K. Kumagai, N. Matsumoto, and S. Nagata, Metal-insulator transition in the spinel $CuIr_2(S_{1-x}Se_x)_4$ system studied by NMR, Phys. C (Amsterdam) **282-287**, 1107 (1997).

[12] E. Maciążek, A. Molak, and T. Goryczka, Influence of cobalt substitution on structure and electric conduction of $CuCr_2Se_4$, J. Alloys Compd. **441**, 222 (2007).

[13] R. Li, Z. Qu, L. Zhang, L. Ling, W. Tong, and Y. Zhang, Structure, magnetic and transport properties of Li-doped $CuCr_2Se_4$, Solid State Commun. **150**, 2289 (2010).

[14] I. Jendrzejewska, P. Zajdel, J. Mroziński, E. Maciążek, T. Goryczka, A. Hanc, and A. Kita, X-ray investigations and magnetic properties of $CuCr_{2-x}Sn_xSe_4$ - compounds, Solid State Phenomena **163**, 208 (2010).

[15] E. Maciążek, E. Malicka, A. Gągor, Z. Stokłosa, T. Groń, B. Sawicki, H. Duda, and A. Gudwański, Semiconducting-metallic transition of singlecrystalline ferromagnetic Hf-doped $CuCr_2Se_4$ spinels, Phys. B (Amsterdam) **520**, 116 (2017).

[16] P. Valencia-Gálvez, O. Peña, S. Moris, and P. Barahona, Raman characterization of $CuCr_{2-x}Sn_xS_4$ spinels, J. Chil. Chem. Soc. **64**, 4285 (2019).

[17] R. Bouchard, Spinel to defect NiAs structure transformation, Mater. Res. Bull. **2**, 459 (1967).

[18] Y. Amiel, G. K. Rozenberg, N. Nissim, A. Milner, M. P. Pasternak, M. Hanfland, and R. D. Taylor, Intricate relationship between pressure-induced electronic and structural transformations in $FeCr_2S_4$, Phys. Rev. B **84**, 224114 (2011).

[19] I. Efthimiopoulos, Z. T. Y. Liu, S. V. Khare, P. Sarin, V. Tsurkan, A. Loidl, D. Popov, and Y. Wang, Structural transition in the magnetoelectric $ZnCr_2Se_4$ spinel under pressure, Phys. Rev. B **93**, 174103 (2016).

[20] I. Efthimiopoulos, V. Tsurkan, A. Loidl, D. Zhang, and Y. Wang, Comparing the pressure-induced structural behavior of $CuCr_2O_4$ and $CuCr_2Se_4$ spinels, J. Phys. Chem. C **121**, 16513 (2017).

[21] T. Saha-Dasgupta, M. De Raychaudhury, and D. D. Sarma, Ferromagnetism in metallic chalcospinels $CuCr_2S_4$ and $CuCr_2Se_4$, Phys. Rev. B **76**, 054441 (2007).

[22] I. Nakatani, H. Nosé, and K. Masumoto, Magnetic properties of $CuCr_2Se_4$ single crystals, J. Phys. Chem. Solids **39**, 743 (1978).

[23] F. Lotgering, Ferromagnetism in spinels: $CuCr_2S_4$ and $CuCr_2Se_4$, Solid State Commun. **2**, 55 (1964).

[24] C. Colominas, Neutron-diffraction investigation of $CuCr_2Se_4$ and $CuCr_2Te_4$, Phys. Rev. **153**, 558 (1967).

[25] M. Ballal and C. Mande, X-ray spectroscopic study of the valency of copper in the spinels $CuCr_2X_4$ ($X$ = O, S, Se, Te), Solid State Commun. **19**, 325 (1976).

[26] O. Yamashita, Y. Yamaguchi, I. Nakatani, H. Watanabe, and K. Masumoto, Polarized neutron diffraction study of a $CuCr_2Se_4$ single crystal, J. Phys. Soc. Jpn. **46**, 1145 (1979).

[27] D. Rodic, B. Antic, R. Tellgren, H. Rundlof, and J. Blanusa, A change of magnetic moment of Cr ion with the magnetic phase transition in $CuCr_2Se_4$, J. Magn. Magn. Mater. **187**, 88 (1998).

[28] A. Kimura, J. Matsuno, J. Okabayashi, A. Fujimori, T. Shishidou, E. Kulatov, and T. Kanomata, Soft x-ray magnetic circular dichroism study of the ferromagnetic spinel-type Cr chalcogenides, Phys. Rev. B **63**, 224420 (2001).

[29] H. Hahn, C. De Lorent, and B. Harder, Untersuchungen über ternäre chalkogenide. VIII. Über die struktur des $CuV_2S_4$, $CuCr_2S_4$, $CuCr_2Se_4$ und $CuCr_2Te_4$, Z. Anorg. Allg. Chem. **283**, 138 (1956).

[30] R. J. Bouchard, P. A. Russo, and A. Wold, Preparation and electrical properties of some thiospinels, Inorg. Chem. **4**, 685 (1965).

[31] K. Oda, S. Yoshii, Y. Yasui, M. Ito, T. Ido, Y. Ohno, Y. Kobayashi, and M. Sato, Unusual anomalous Hall resistivities of $CuCr_2S_4$, $Cu_{0.5}Zn_{0.5}Cr_2Se_4$ and $Cr_3Te_4$, J. Phys. Soc. Jpn. **70**, 2999 (2001).

[32] P. Barahona, A. Galdámez, F. López-Vergara, V. Manríquez, and O. Peña, Crystal structure and magnetic properties of titanium-based $CuTi_{2-x}M_xS_4$ and $CuCr_{2-x}Ti_xSe_4$ chalcospinels, J. Solid State Chem. **212**, 114 (2014).

[33] C. Pinto, A. Galdámez, P. Barahona, S. Moris, and O. Peña, Crystal structure, Raman scattering and magnetic properties of $CuCr_{2-x}Zr_xSe_4$ and $CuCr_{2-x}Sn_xSe_4$ selenospinels, J. Magn. Magn. Mater. **456**, 160 (2018).

[34] S. Moris, P. Valencia-Gálvez, J. Mejía-López, O. Peña, P. Barahona, and A. Galdámez, $(Cu)_{tet}(Cr_{2-x}Sn_x)_{oct}S_{4-y}Se_y$ spinels: Crystal structure, density functional theory calculations, and magnetic behavior, Inorg. Chem. **58**, 13945 (2019).

[35] J. Rodríguez-Carvajal, Recent advances in magnetic structure determination by neutron powder diffraction, Phys. B (Amsterdam) **192**, 55 (1993).

[36] M. I. Aroyo, J. M. Perez-Mato, D. Orobengoa, E. Tasci, G. de la Flor, and A. Kirov, Crystallography online: Bilbao crystallographic server, Bulg. Chem. Commun. **43**, 183 (2011).

[37] M. I. Aroyo, J. M. Perez-Mato, C. Capillas, E. Kroumova, S. Ivantchev, G. Madariaga, A. Kirov, and H. Wondratschek, Bilbao crystallographic server: I. Databases and crystallographic computing programs, Z. Kristallogr.-Cryst. Mater. **221**, 15 (2006).

[38] M. I. Aroyo, A. Kirov, C. Capillas, J. M. Perez-Mato, and H. Wondratschek, Bilbao crystallographic server. II. Representations of crystallographic point groups and space groups, Acta Crystallogr. Sect. A **62**, 115 (2006).

[39] J. Perez-Mato, S. Gallego, E. Tasci, L. Elcoro, G. de la Flor, and M. Aroyo, Symmetry-based computational tools for magnetic crystallography, Annu. Rev. Mater. Res. **45**, 217 (2015).

[40] A. I. Abramovich, L. I. Koroleva, and L. N. Lukina, Spin-glass and reentrant spin-glass states in iron sulfospinels having dilute $A$ and $B$ sublattices, Phys. Solid State **41**, 73 (1999).

[41] Y. Iijima, Y. Kamei, N. Kobayashi, J. Awaka, T. Iwasa, S. Ebisu, S. Chikazawa, and S. Nagata, A new ferromagnetic thiospinel $CuCrZrS_4$ with re-entrant spin-glass behaviour, Philos. Mag. **83**, 2521 (2003).

[42] K. Belakroum, Z. Ouili, A. Leblanc-Soreau, M. Hemmida, and H.-A. Krug von Nidda, Magnetic properties of CuCrZrSe4, J. Magn. Magn. Mater. **334**, 130 (2013).

[43] R. D. Shannon, Revised effective ionic radii and systematic studies of interatomic distances in halides and chalcogenides, Acta Crystallogr. Sect. A **32**, 751 (1976).

[44] E. Riedel and W. Morlock, Spinelle mit substituierten Nichtmetallteilgittern. VI. Röntgenographische und elektronische Eigenschaften, Mößbauer- und IR-spektren des spinellsystems $CuCrSn(S_{1-x}Se_x)_4$, Z. Anorg. Allg. Chem. **438**, 233 (1978).

[45] D. Mähl, J. Pickardt, and B. Reuter, Züchtung und untersuchung von einkristallen der verbindungen $CuCrZrSe_4$ und $CuCrSnSe_4$, Z. Anorg. Allg. Chem. **508**, 197 (1984).

[46] P. Valencia-Gálvez, D. Aravena, P. Barahona, S. Moris, and A. Galdámez, Effects of tin and sulfur chemical substitution on the structural and electrical properties of $CuCr_2Se_4$ selenospinel, Appl. Sci. **12**, 1586 (2022).

[47] A. V. Powell, P. Vaqueiro, K. S. Knight, L. C. Chapon, and R. D. Sánchez, Structure and magnetism in synthetic pyrrhotite $Fe_7S_8$: A powder neutron-diffraction study, Phys. Rev. B **70**, 014415 (2004).

[48] D. Fiorani, L. Gastaldi, A. Lapiccirrella, S. Viticoli, and N. Tomassini, Monte Carlo simulation of percolative phenomena in the cationic $B$-sublattice of spinels, Solid State Commun. **32**, 831 (1979).

[49] J. R. L. d. Almeida and D. J. Thouless, Stability of the Sherrington-Kirkpatrick solution of a spin glass model, J. Phys. A: Math. Gen. **11**, 983 (1978).

[50] M. Gabay and G. Toulouse, Coexistence of spin-glass and ferromagnetic orderings, Phys. Rev. Lett. **47**, 201 (1981).

[51] C. Rao and K. Pisharody, Transition metal sulfides, Prog. Solid State Chem. **10**, 207 (1976).